Earth and Planetary Science Letters 432 (2015) 46–58

Contents lists available at ScienceDirect

Earth and Planetary Science Letters

www.elsevier.com/locate/epsl

A high-resolution record of Southern Ocean intermediate water radiocarbon over the past 30,000 years

Sophia K.V. Hines [a,*], John R. Southon [b], Jess F. Adkins [a]

[a] California Institute of Technology, Department of Geological and Planetary Science, 1200 E California Blvd., MC 131-24, Pasadena, CA 91125, United States
[b] University of California Irvine, Department of Earth System Science, Irvine, CA 92697, United States

ARTICLE INFO

Article history:
Received 5 February 2015
Received in revised form 8 September 2015
Accepted 24 September 2015
Available online 3 November 2015
Editor: H. Stoll

Keywords:
Southern Ocean
radiocarbon
glacial–interglacial climate change
meridional overturning circulation
Southern Ocean fronts
intermediate water

ABSTRACT

The circulation of intermediate waters plays an important role in global heat and carbon transport in the ocean and changes in their distribution are closely tied to glacial–interglacial climate change. Coupled radiocarbon and U/Th measurements on deep-sea *Desmophyllum dianthus* corals allow for the reconstruction of past intermediate water ventilation. We present a high-resolution time series of Antarctic Intermediate Water radiocarbon from 44 corals spanning 30 ka through the start of the Holocene, encompassing the transition into the Last Glacial Maximum (LGM) and the last deglaciation. Corals were collected south of Tasmania from water depths between 1430 and 1950 m with 80% of them between 1500 and 1700 m, giving us a continuous record from a narrow depth range. The record shows three distinct periods of circulation: the MIS 3–2 transition, the LGM/Heinrich Stadial 1 (extending from ~22 to 16 kyr BP), and the Antarctic Cold Reversal (ACR). The MIS 3–2 transition and the ACR are characterized by abrupt changes in intermediate water radiocarbon while the LGM time period generally follows the atmosphere at a constant offset, in support of the idea that the LGM ocean was at steady state for its ^{14}C distribution. Closer inspection of the LGM time period reveals a 40‰ jump at ~19 ka from an atmospheric offset of roughly 230‰ to 190‰, coincident with an observed 10–15 m rise in sea level and a southward shift of the Subantarctic and Polar Fronts, an abrupt change not seen in deeper records. During the ACR time period intermediate water radiocarbon is on average less offset from the atmosphere (~110‰) and much more variable. This variability has been captured within the lifetimes of three individual corals with changes of up to 35‰ over ~40 yr, likely caused by the movement of Southern Ocean fronts. This surprising result of relatively young and variable intermediate water radiocarbon during the ACR seems to go against the canonical idea of reduced circulation and ventilation in the south during this time period. However comparisons with other records from the Southern Ocean highlight zonal asymmetries, which can explain the deviation of our Tasmanian record from those in Drake Passage and the eastern Pacific. These signals seen in Tasmanian intermediate water $\Delta^{14}C$ can also be found in Greenland ice core $\delta^{18}O$ and East Asian monsoon strength. Throughout the LGM and the deglaciation, our Tasmanian intermediate water record is sensitive to times when the upper and lower cells of the meridional overturning circulation are more or less interconnected, which has important implications for the global climate system on glacial–interglacial time scales.

1. Introduction

The ocean is an important driver of global climate on a variety of timescales. Water has a large heat capacity, which allows the oceans to transport significant amounts of sensible heat from the tropics to the poles. Relative to its volume transport, intermediate water carries a large amount of heat due to the large temperature difference between its formation and upwelling regions (Talley, 2013, 2003). In addition to the ocean's direct effect on climate through heat transport, the deep ocean stores 60 times more carbon than the atmosphere, so changes in ocean circulation can have dramatic impacts on the global carbon cycle. Carbon is stored in the deep ocean via the biological, solubility, and alkalinity pumps, and deeply regenerated CO_2 returns to the atmosphere when deep water upwells to the surface as part of the meridional overturning circulation (Hain et al., 2014; Sigman et al., 2010).

One important tracer that is useful both for reconstructing mean and local ocean circulation is radiocarbon. Radiocarbon (^{14}C)

* Corresponding author. Tel.: +1 626 395 8649.
E-mail address: shines@caltech.edu (S.K.V. Hines).

http://dx.doi.org/10.1016/j.epsl.2015.09.038
0012-821X/

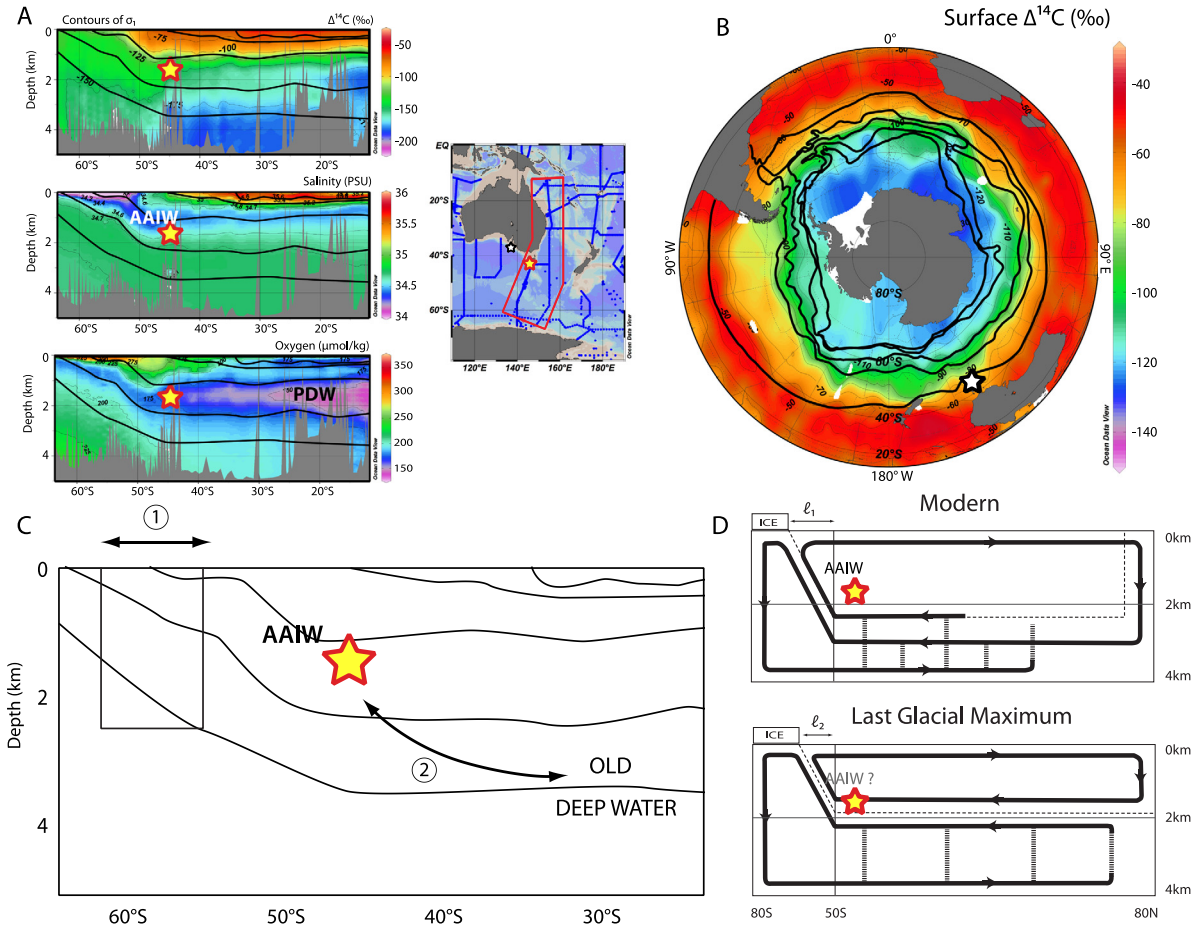

Fig. 1. Hydrography for the broader region around our sample location. A) Sections of bomb-corrected Δ^{14}C (top), salinity (middle), and oxygen (bottom) from ~65°S to 10°S for the region marked on the inset map (Key et al., 2004). Sample location marked with a yellow star. Thick black contour lines are isopycnals (σ_1). In this region, tracers largely move along density surfaces. Map to the right shows the location of the sections, the Tasmanian coral location (yellow star) and the location of core MD-03-2611 (black star). B) Surface map of bomb-corrected Δ^{14}C for the whole Southern Ocean. Thick black lines mark the positions of the major Southern Ocean fronts (from furthest north to furthest south: Subtropical Front (STF), Subantarctic Front (SAF), Polar Front (PF), Southern ACC Front (SACCF), and the Southern Boundary (SB)). C) Schematic Southern Ocean section with contours of density (taken from panel A). Coral location is marked with yellow star, and arrows show the two main ways to change radiocarbon values. D) Schematic of modern and glacial meridional overturning circulation with coral location marked with yellow star (adapted from Ferrari et al., 2014). In the modern, upper and lower cells are intertwined whereas in the glacial, cells are separated. This is due to increased sea ice extent (note: ℓ_1 in the upper panel is greater than ℓ_2 in the lower panel). (For interpretation of the references to color in this figure legend, the reader is referred to the web version of this article.)

is cosmogenically produced in the atmosphere where it is quickly converted to $^{14}CO_2$. Its 5730-yr half-life makes ^{14}C well suited as a tracer for deep ocean circulation, which occurs on time scales of ~1000 yr. The rate of change of radiocarbon in the atmosphere is a balance between ^{14}C production (which is variable in time), exchange with the ocean, and self-decay, which makes the radiocarbon value of the atmosphere a very sensitive recorder of globally integrated ocean overturning. Reconstructions of ^{14}C production through time (Hain et al., 2014; Laj et al., 2002; Muscheler et al., 2004) are helpful for disentangling these competing processes that imprint themselves on atmospheric Δ^{14}C. However, production rate records are difficult to generate. Although mean ocean circulation changes can help explain global shifts in climate, the specific regions involved and the timing of regional changes is also crucial for understanding the mechanisms at work. Measurements of radiocarbon in the ocean are therefore important because they provide local information that can be combined with the atmospheric record to generate a global understanding of how the ocean behaves over millennial timescales.

We provide an intermediate water Δ^{14}C reconstruction from south of Tasmania in the Indo-Pacific region of the Southern Ocean (Fig. 1). In the modern ocean, Antarctic Intermediate Water (AAIW) ventilates this region between ~500 and 1500 m. Intermediate waters are defined by extrema in salinity, and AAIW can be easily seen in the middle panel of Fig. 1A as the tongue of low-salinity water extending from the surface of the Southern Ocean to between ~500–1500 m. At the sample location this water has a bomb-corrected Δ^{14}C value of around −150‰ (Fig. 1A, top panel), and underlying Circumpolar Deep Water (CDW) and Antarctic Bottom Water (AABW) are more depleted in radiocarbon. The core of Pacific Deep Water is marked by an oxygen minimum (Talley, 2013), and its return flow to the Southern Ocean intersects with our sample location (Fig. 1A, bottom panel). As Talley points out, the modern meridional overturning circulation (MOC) does not consist of two separate cells stacked on top of one another; instead both cells are intertwined (Fig. 1D, top panel).

Through the application of simple box models, it has been shown that increasing the meridional overturning strength and reducing the efficiency of the biological pump together are able to accomplish the full glacial to interglacial CO_2 change (Knox and McElroy, 1984; Sarmiento and Toggweiler, 1984; Siegenthaler and Wenk, 1984). The configuration of the ocean during the Last Glacial Maximum (LGM) was distinct from the modern (Curry and Oppo, 2005), and it is thought that the ocean circulation was near steady state during this time. Benthic carbon and oxygen isotope measurements show a shoaling of the boundary between the northern

and southern source water masses and a sharper gradient between them (Curry and Oppo, 2005; Lund et al., 2011). Recently, a mechanism has been proposed to move between the interglacial and glacial circulation schemes. It builds on the observation that the boundary between the upper and lower cells is defined by the switch between positive and negative buoyancy forcing at the surface of the Southern Ocean, and that this location generally aligns with the summertime sea ice edge (Ferrari et al., 2014). To first order, isopycnals have a constant slope across the Southern Ocean and are flat in the rest of the ocean basin, so it is possible to calculate the depth of the boundary between deep cells based on the high latitude buoyancy forcing. In the modern ocean, this boundary sits at around 2200 m, which is deep enough for the rough topography at the bottom of the ocean to effectively mix water between the cells. Expanded sea ice during the LGM shoals this boundary out of the rough region and allows for separation between the upper and lower cells (Fig. 1D) (Ferrari et al., 2014).

In this paper, we use the results of age screening deep-sea corals from the Caltech collection to select samples for a continuous well-dated time series of $\Delta^{14}C$ from a narrow depth range in the region south of Tasmania. This high-resolution time series is then used to examine glacial climate and the behavior of the Southern Ocean during the deglaciation. Our sample location lies within the modern and glacial upper cell but near its lower boundary, so it is quite sensitive to the interconnectedness of the meridional overturning circulation. We assess this interconnectedness by comparing our Tasmanian intermediate water $\Delta^{14}C$ record to other Southern Ocean records from different depths as well as atmospheric CO_2.

2. Methods

Deep-sea corals used in this study were collected from seamounts south of Tasmania (43°S–47°S 144°E–152°E) during cruise TN-228 in 2008–2009 on the R/V Thompson using the remotely operated deep submergence vehicle JASON. During this cruise over 10,000 deep-sea corals were collected from between 898–2395 m. All corals used for the construction of this time series were the scleractinian azooxanthellate *Desmophyllum dianthus*. The time series presented here encompasses samples from 1430–1950 m with 80% of samples between 1500 and 1700 m (marked with a star in Fig. 1A sections).

Previous reconnaissance radiocarbon dating (Thiagarajan et al., 2013) was performed at the National Ocean Sciences Accelerator Mass Spectrometry Laboratory at the Woods Hole Oceanographic Institute following the method of Burke et al. (2010) using an Elemental Analyzer. Additional radiocarbon age screening was performed at the UC Irvine Keck Carbon Cycle AMS facility following the 'rapid survey' method of Bush et al. (2013). Reconnaissance ^{14}C dates were converted into calendar ages using IntCal13 and the Calib 7.0 software and reservoir age offsets according to Thiagarajan et al. (2013) for consistency (1250 yr for the Holocene and 1900 yr for all samples older than 10 kyr).

In preparation for U/Th and high-precision radiocarbon dating, all coral samples were physically and chemically cleaned following previously established methods (Cheng et al., 2000; Shen and Boyle, 1988). U/Th dating was performed using previously established methods (Cheng et al., 2000; Robinson et al., 2007). Approximately 100 mg of coral was weighed, dissolved in Seastar HNO_3, and spiked with a mixed ^{229}Th–^{236}U spike. Uranium and thorium were separated from the rest of the coral matrix by iron co-precipitation and anion exchange chromatography. Purified U and Th fractions were dried and re-dissolved in 5% Seastar nitric acid and measured on a Thermo Scientific Neptune MC-ICPMS. Bracketing CRM-145 standards for uranium and SGS standards for thorium were used to correct for instrumental drift, mass bias and gain. Uranium samples were intensity matched to within ~10% of the CRM-145 standard for ^{234}U, which was measured on the center position secondary electron multiplier with a retarding potential quadruple to reduce scattered ion effects. ^{235}U, ^{236}U, and ^{238}U were measured on Faraday cups with 10^{11} ohm resistors. ^{229}Th and ^{230}Th were measured on channeltron ion counters and ^{232}Th was measured on a Faraday cup with a 10^{11} ohm resistor. Four procedural blanks were run with each set of samples and the average of the blank values was subtracted from each of the samples. Samples and standards were also corrected for instrumental blank using the average of bracketing 5% Seastar nitric used to dilute samples and standards. Samples were corrected for initial thorium using a $^{230}Th/^{232}Th$ atom ratio of $80 \pm 80 \times 10^{-6}$ (Cheng et al., 2000).

High-precision ^{14}C dating was performed at the Keck Carbon Cycle AMS facility at UC Irvine. Approximately 11 mg of cleaned coral was weighed into a 3 mL rubber septum top vial and leached in 0.01% HCl to remove 10% of the coral mass. Samples were then dried, evacuated and hydrolyzed in phosphoric acid. The resulting CO_2 was purified and graphitized with H_2 and an iron catalyst (Santos et al., 2007). Graphite was pressed into aluminum targets for ^{14}C analysis on the accelerator mass spectrometer. Measured radiocarbon activities are normalized for mass-dependent fractionation using $\delta^{13}C$ values measured on the AMS, and normalized to a $\delta^{13}C_{PDB}$ value of −25‰. Radiocarbon activities are reported as fraction modern (F_m) relative to 95% of the activity of NBS oxalic acid standard in the year 1950 (normalized to $\delta^{13}C_{PDB} = -19‰$). Fraction modern is converted to a ^{14}C age using the formula ^{14}C age $= -8033 \ln(F_m)$. Radiocarbon blanks measured on ^{14}C-dead deep-sea corals tend to be larger and more variable than those measured on ^{14}C-dead calcite (e.g. Adkins et al., 2002; Eltgroth et al., 2006). Therefore, corals are background corrected using the average and standard deviation of radiocarbon values measured on replicate samples ($n = 8$) of a "radiocarbon dead" deep-sea coral ($F_m = 0.0034 \pm 0.0007$) with a U/Th age of $205{,}000 \pm 3000$ yr.

Intermediate water $\Delta^{14}C$ values were reconstructed using measured U/Th ages and high-precision radiocarbon dates on coral samples according to the expression:

$$\Delta^{14}C = \left(\frac{e^{-^{14}C \text{ age/Libby Mean Life}}}{e^{-U/Th \text{ age/True Mean Life}}} - 1 \right) \times 1000$$

where the Libby Mean Life is 8033 yr and the True Mean Life is 8266 yr (Stuiver and Polach, 1977). This $\Delta^{14}C$ value corrects for the time elapsed since each coral sample grew, thereby extracting the $\Delta^{14}C$ value of the water it grew in, relying on the assumption that both the carbon isotope system and the U/Th isotope system have remained closed. For corals with top, middle, and bottom dates, a single U/Th age is measured on the top of the coral and middle and bottom dates are inferred using measured distances between subsamples and a growth rate of 1 mm/yr (Adkins et al., 2004). Age errors for middle and bottom subsamples are assigned to be 50 yr. Error in the $\Delta^{14}C$ value incorporates both error from U/Th dating and ^{14}C dating. Because calculating $\Delta^{14}C$ involves taking a ratio of exponentials, error in either of the dates can cause the total error to greatly increase (Supplemental Fig. 1). When comparing these intermediate water $\Delta^{14}C$ values to the contemporaneous atmosphere, it is most appropriate to transform the $\Delta^{14}C$ data into epsilon values, which are similar to $\Delta\Delta^{14}C$. Epsilon values are the proper way of differencing delta values and are calculated by converting the $\Delta^{14}C$ of each sample and the contemporaneous atmosphere into ratios, and taking the ratio of the ratios:

$$\varepsilon = \left(\left[\frac{\frac{\Delta^{14}C_{sample}}{1000} + 1}{\frac{\Delta^{14}C_{atm}}{1000} + 1} \right] - 1 \right) \times 1000$$

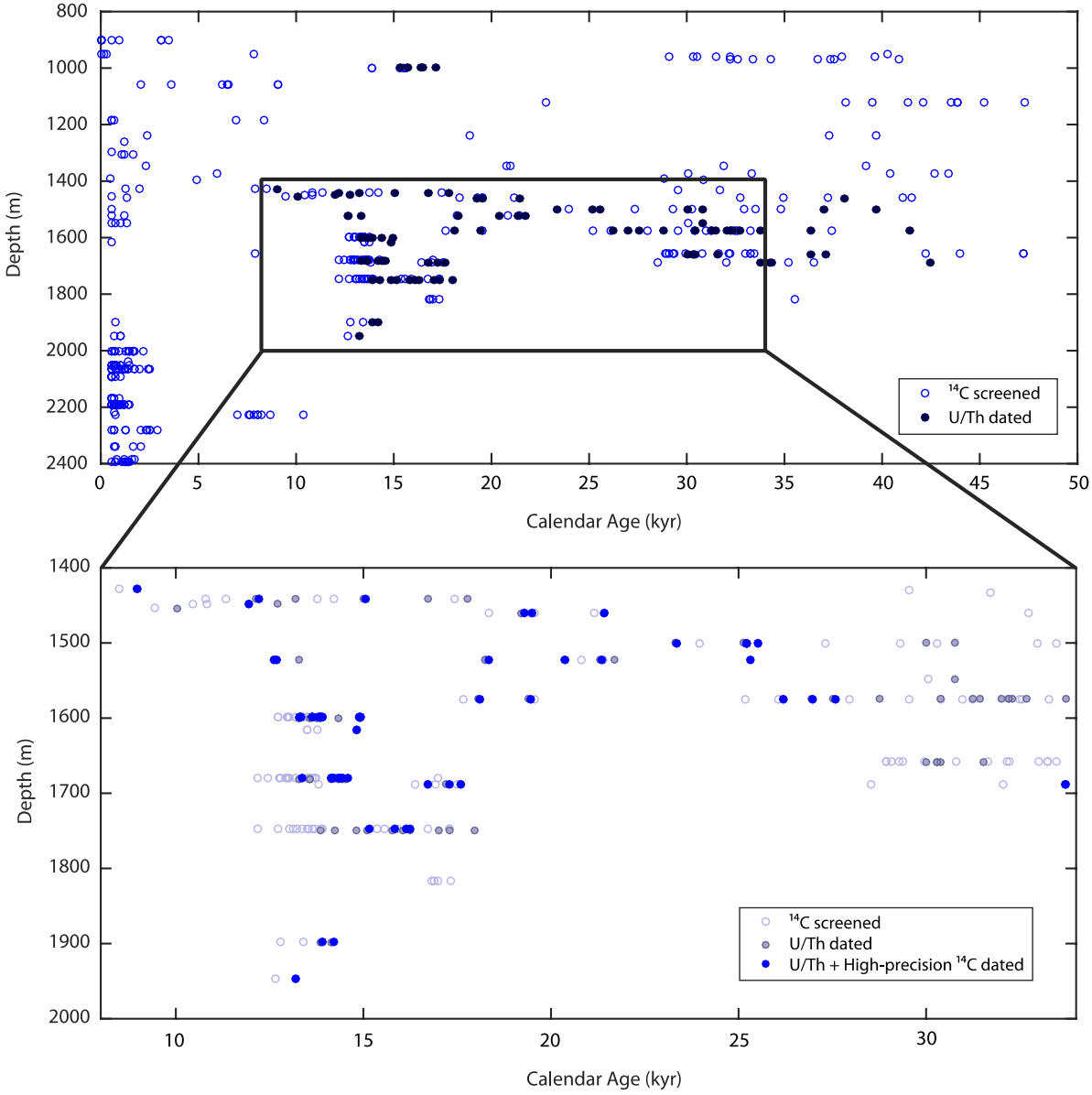

Fig. 2. Age-depth distribution for ^{14}C screened corals. Upper panel shows all screened corals (blue open circles; $n = 508$) and individuals that were selected for U/Th dating (blue filled circles; $n = 112$). Lower panel is an expanded view of the boxed region in the upper panel. In the lower panel, ^{14}C screened and U/Th dated corals from the upper panel are shown in lighter blue, and filled blue circles represent the subset of U/Th dated samples that were also high-precision ^{14}C dated ($n = 44$). (For interpretation of the references to color in this figure legend, the reader is referred to the web version of this article.)

Epsilon is a more correct measure of past ocean circulation changes than $\Delta\Delta^{14}$C because it takes into account changes in atmospheric Δ^{14}C value itself. It is therefore the parameter that stays constant (for sufficiently slow ^{14}C production changes) if ocean circulation does not change.

3. Results

Radiocarbon age screening reveals patterns consistent with those published by Thiagarajan et al. (2013) (Fig. 2). 97 corals were selected for ^{14}C screening from between 1390–1748 m, and 162 corals were selected from between 2004–2739 m. Previously, an additional 249 samples from between the depths of 899–2395 m were measured by Thiagarajan et al. (2013). All of the corals deeper than 2000 m are Holocene-age with most younger than 5000 yr. There is an abundance peak with a greater depth range (1450–1950 m) that roughly coincides with the ACR and HS1. The LGM on the other hand has a much more restricted depth range, with most corals between 1450–1575 m. Average uncertainties were 300 ^{14}C-yr for samples screened at NOSAMS using the EA method, and 500 ^{14}C-yr for samples screened at UC Irvine using the 'rapid survey' method. The average offset between screened ages (converted into calendar age) and U/Th ages is 1500 yr. This discrepancy is most likely the result of our choice of reservoir age through time, in addition to changes in ventilation age.

In order to have a sufficient age range and sampling frequency for the Δ^{14}C time series, 103 individual corals were U/Th dated (Supplementary Table 1). Samples were selected for U/Th dating based on their depth and reconnaissance age. Dates were assessed based on two main criteria: the amount of ^{232}Th, which increases errors due to uncertainty in the initial ^{232}Th/^{230}Th ratio, and the initial δ^{234}U value, which provides information about whether or not the sample has behaved as a closed system (a primary assumption for U/Th dates). If the sample has behaved as a closed system, then the calculated initial δ^{234}U ($\delta^{234}U_{init} = \delta^{234}U_{meas}e^{\lambda t}$) should be within error of the marine δ^{234}U value. 14 samples had ^{232}Th

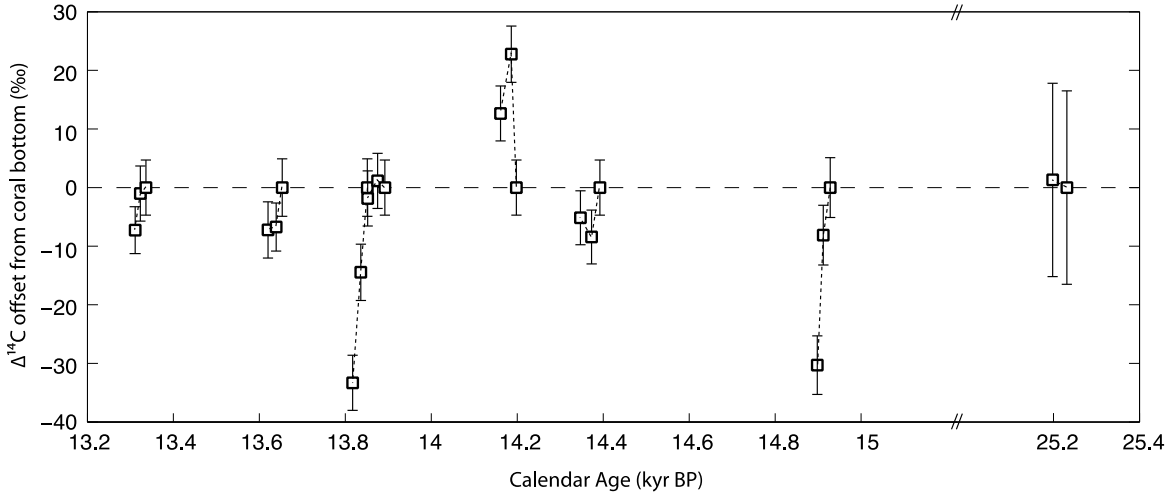

Fig. 3. Changes in $\Delta^{14}C$ over the lifetime of single deep-sea coral specimens. Seven corals were sub-sampled for top–middle–bottom ^{14}C dates and one for top–bottom ^{14}C dates. Calculated $\Delta^{14}C$ values are plotted as differences from the bottom of the coral with 1σ error bars based only on uncertainty from radiocarbon dating. Of these eight corals, three show distinguishable changes in $\Delta^{14}C$ over the lifetime of the coral, two show no change, and three show slight changes that are not resolvable within error. (Note break in *x*-axis between 15 and 25.2 ka.)

concentrations above the cutoff value of 2000 ppt, and 3 samples had $\delta^{234}U_{init}$ values that were non-marine using the selection criteria from IntCal09, which is defined as 147 ± 7‰ for corals younger than 17 kyr and 141.7 ± 7.8‰ for corals older than 17 kyr (Reimer et al., 2009). The average relative error for all dates was 6.64‰ and the average relative error for all samples that met the ^{232}Th and $\delta^{234}U$ criteria was 5.26‰. Procedural blanks account for 0.05% or less of the total error for ^{238}U and ^{234}U, 0.14% of the total error for ^{230}Th, and 1.97% of the total error for ^{232}Th, with average values of 38 fmol for ^{232}Th and 0.29 pmol for ^{238}U.

Out of the 103 individual corals that were U/Th dated, 44 were selected for high-precision radiocarbon dating. Keeping with the goal of creating a high-resolution continuous time series, samples were selected for high-precision radiocarbon dating based on their U/Th ages, ^{232}Th concentrations, and uranium isotope values. Of these 44 samples, eight were subsampled for top, middle, and bottom dates (Fig. 4). Average relative errors radiocarbon dates were 2.7‰ for samples less than 15,000 ^{14}C-yr, 3.6‰ for samples between 15,000–20,000 ^{14}-yr, 4.6‰ for samples between 20,000–25,000 ^{14}C-yr, and 8.4‰ for samples older than 25,000 ^{14}C-yr.

The $\Delta^{14}C$ dataset presented here is the highest resolution record that has been produced for this time in the Southern Ocean. It contains 68 ^{14}C dates on 44 individual corals between 9000–33,790 yr with an average sampling resolution of 575 yr (average resolution of 295 yr between 9000–15,170 yr and 590 yr between 15,830–27,580 yr) (Fig. 3). Eight of these 44 corals were also subsampled for even higher resolution radiocarbon dating during times of increased $\Delta^{14}C$ variability, and three of these corals reveal resolvable changes in intermediate water radiocarbon occurring on decadal timescales (Fig. 3; depicted as separate $\Delta^{14}C$ points connected by lines on subsequent figures).

The full record can be broken up into three main segments based on chronology and $\Delta^{14}C$ behavior during these periods: the Marine Isotope Stage (MIS) 3–2 transition, the LGM/early HS1, and the ACR. The MIS 3–2 transition segment is characterized by one large drop in intermediate water radiocarbon of ~ 250‰ starting at 27.6 ka. This drop is followed by a period of intermediate water variability and then a gap between 23.6–21.5 ka. Between 21.5–16 ka, the LGM/early HS1 segment, intermediate waters roughly follow the atmosphere with an offset of around 200‰ (with a ~40‰ jump at around 19 ka). Then there is an 800-yr gap in the record, after which intermediate waters are on average less offset from the atmosphere but far more variable. This final ACR segment contains three corals that record abrupt changes in intermediate radiocarbon within their lifetimes. There is a drop of 30‰ at 14.9 ka, a rise of 23‰ at 14.2 ka, and a drop of 35‰ at 13.9 ka (Fig. 3 and Fig. 4).

4. Discussion

The Southern Ocean is a region where deep water upwells to the surface and exchanges with the atmosphere making it important to global climate. The Southern Ocean is also important in setting atmospheric CO_2 values over glacial–interglacial timescales (Sarmiento and Toggweiler, 1984). In the Southern Ocean, surface $\Delta^{14}C$ values are generally aligned with isopycnals and fronts (Fig. 1B). This is the result of Southern Ocean overturning, where the oldest water upwells close to Antarctica, and the residence time of water at the surface, which is not long enough for the full exchange of carbon isotopes. This leads to a meridional surface gradient in $\Delta^{14}C$ with more negative values closest to Antarctica (Fig. 1B). When water leaves the surface of the Southern Ocean, the surface $\Delta^{14}C$ gradient is transformed into a vertical gradient (Fig. 1A). Because of this pattern, there are two main mechanisms to generate changes in intermediate water $\Delta^{14}C$ at our sampling location—one of them able to produce abrupt changes on annual to decadal timescales and the other tending to produce more gradual changes over centennial to millennial timescales (Fig. 1C). On short timescales, meridional shifts in the position of Southern Ocean fronts can change the $\Delta^{14}C$ value of the water ventilating a particular region (Fig. 1C; mechanism 1). On longer timescales, $\Delta^{14}C$ changes could also reflect the degree of mixing between Tasmanian intermediate water and older Pacific deep water below and to the north (Fig. 1C; mechanism 2). The amount of mixing between Tasmanian intermediate water and older, deeper water masses also dictates how responsive intermediate waters will be to changes in atmospheric CO_2, since older deep waters carry the majority of regenerated CO_2. In general, the positions of fronts in the Southern Ocean are dictated by bathymetry (Graham et al., 2012). However in the absence of strong bathymetric features, fronts are less constrained and respond to the position of Southern Ocean westerly winds (Sallée et al., 2008). This latter scenario is the case for the Subantarctic and Polar Fronts in the region south of Tasmania, between which Antarctic Intermediate Water is formed.

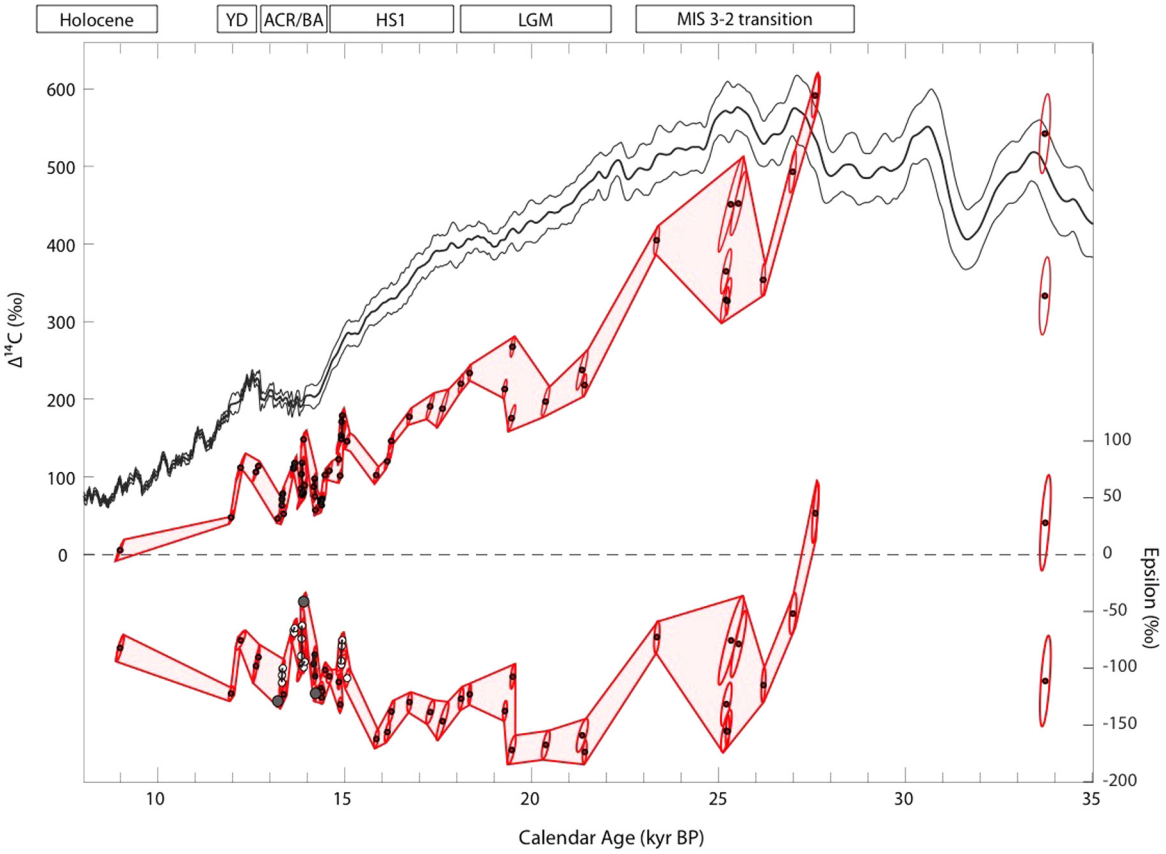

Fig. 4. A) Tasmanian $\Delta^{14}C$ record plotted with IntCal13 atmospheric $\Delta^{14}C$ record, and B) converted into epsilon values. Error ellipses represent 1σ correlated U/Th and $\Delta^{14}C$ errors. For epsilon values, these ellipses also take into account uncertainty in the IntCal13 atmospheric $\Delta^{14}C$ record. Despite coming from between 1442 and 1947 m, epsilon variability between ~15–13 ka is not depth dependent. The deepest samples (at 1947 and 1898 m) are shown in panel B with dark gray filled circles, and they encompass nearly the full range in epsilon (including the highest point). The shallowest samples (at 1442 and 1599 m) are shown with white circles. 25 of the 30 samples from this time interval come from depth range of less than 100 m (1599–1680 m).

4.1. LGM steady state and early frontal shifts

Beginning at 21.5 ka, the Tasmanian coral $\Delta^{14}C$ record generally follows the atmosphere at a constant offset. This trend can be easily seen by converting the $\Delta^{14}C$ record into epsilon units. Between ~21.5 and 19 ka, intermediate waters have an epsilon of ~−170‰. After an abrupt jump of ~40‰ at 19 ka, intermediate water $\Delta^{14}C$ continues to follow the atmosphere, now with epsilon values of around −130‰. Correcting the IntCal13 atmospheric $\Delta^{14}C$ reconstruction for the contribution from production rate changes, the residual atmospheric $\Delta^{14}C$ is flat across most of the LGM, consistent with an ocean–atmosphere system at steady state (Hain et al., 2014) (Fig. 5A). Together, the consistency between the atmosphere and the coral $\Delta^{14}C$ and the constant value of production-corrected atmospheric $\Delta^{14}C$ imply that the ocean was at or near steady state during the LGM.

The jump in intermediate water radiocarbon at ~19 ka is a conspicuous departure from the otherwise steady–state-like conditions of the LGM. This timing is coincident with 10–15 m of sea level rise measured using a series of sediment cores off the northern coast of Australia (Yokoyama et al., 2000). It also corresponds to an abrupt and permanent poleward shift of the Subantarctic (SAF) and Polar Fronts (PF) as shown by foram faunal assemblage data from a core located south of Australia (MD03-2611, 36°43.8′S, 136°32.9′E, 2420 m; Fig. 5D) (De Deckker et al., 2012). A southward shift of the Subantarctic and Polar Fronts would lead to a rise in intermediate water $\Delta^{14}C$ south of Tasmania. The decrease in subpolar foraminifera beginning at 19 ka also marks the first appearance of subtropical fauna, which dominate the rest of the deglaciation.

Based on the relative timing of Northern and Southern Hemisphere ice sheet and mountain glacier retreat following the Last Glacial Maximum, it is thought that the sea level rise at ~19 ka originated from ice sheet retreat in the north (Clark et al., 2009). This influx of fresh water to the North Atlantic caused a reduction in the strength of the Atlantic meridional overturning circulation (AMOC) and initiated warming in the Southern Hemisphere via the bipolar seesaw (Broecker, 1998; Shakun et al., 2012). Atmospheric models show that the ITCZ and other aspects of tropical circulation responds to changes in extratropical temperature, shifting toward the warmer hemisphere (Kang et al., 2008). Shifts in the position of the ITCZ can in turn affect other atmospheric wind belts, shifting them in the same direction (Ceppi et al., 2013). This is consistent both with our $\Delta^{14}C$ record and with foram assemblages from south of Australia (De Deckker et al., 2012). Our data is consistent with melting of Northern Hemisphere ice sheets reducing the strength of the AMOC, which shifted atmospheric winds to the south and caused a southward shift in Southern Ocean fronts.

Although this initial pulse of meltwater at ~19 ka prompts a shift in Tasmanian intermediate water $\Delta^{14}C$, the bulk of the carbon system stays in steady state through this interval, as indicated by the production-corrected IntCal13 record and atmospheric CO_2. The deep ocean exerts the strongest influence on the $\Delta^{14}C$ value of the atmosphere and CO_2 because it is old and contains a large volume of regenerated CO_2. The disconnect between intermediate water $\Delta^{14}C$ and atmospheric $\Delta^{14}C$ at ~19 ka indicates that deep and intermediate waters are not acting together and the upper and lower circulation cells are separate.

Early in the deglaciation atmospheric CO_2 begins to rise as recorded in the Epica Dome C and WAIS divide ice cores (at

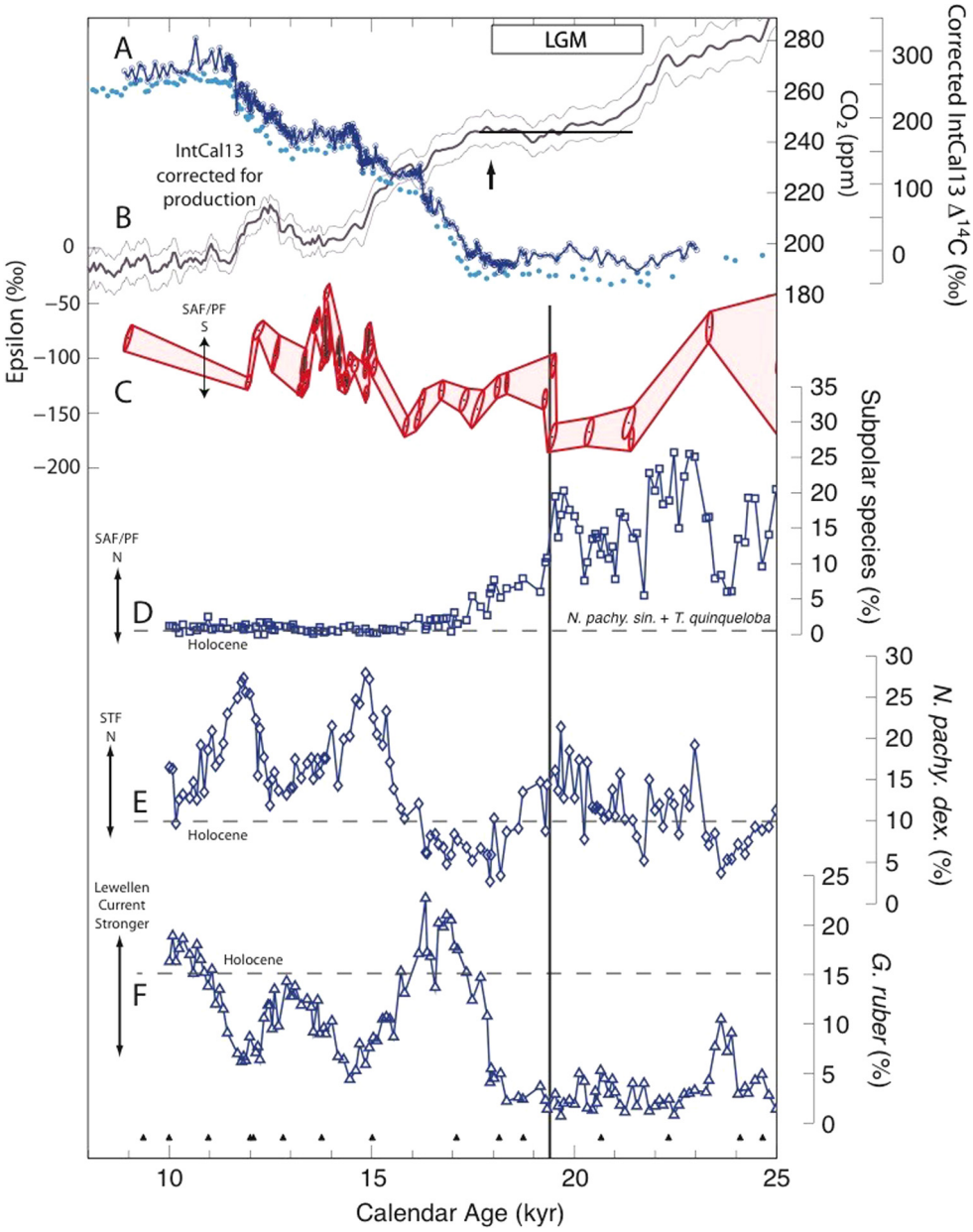

Fig. 5. $\Delta^{14}C$ changes and frontal movement in the Southern Ocean. A) Atmospheric CO_2 curves from EPICA Dome C (through 22 ka) on the timescale of Lemieux-Dudon and Taylor Dome (20–25 ka) (Indermühle et al., 2000; Lemieux-Dudon et al., 2010; Monnin et al., 2001) (light blue dots) and WAIS (Marcott et al., 2014) (dark blue circles and line) B) The IntCal13 atmospheric $\Delta^{14}C$ reconstruction corrected for changes in atmospheric ^{14}C production (Hain et al., 2014). Arrow at top marks the initiation of CO_2 rise at ~18 ka. C) The Tasmanian coral $\Delta^{14}C$ record, converted into epsilon. D–F) Foraminiferal species assemblages from core MD03-2611 (36°43.8′S, 136°32.9′E; 2420 m) located south of Australia (De Deckker et al., 2012). D) Percent abundance of subpolar foraminiferal species assemblage (*N. pachyderma sinestral* and *T. quinqueloba*), indicative of SAF/PF movement. E) *N. pacyderma dextral* percent abundance, indicative of STF movement. F) *G. ruber* percent abundance, representative of the strength of the Lewellen Current. Black triangles at the bottom of the figure are age control points for MD03-2611 based on calibrated ^{14}C ages. (For interpretation of the references to color in this figure legend, the reader is referred to the web version of this article.)

~17.5 ka according to EDC and ~18 ka according to WAIS) (Fig. 5A) (Lemieux-Dudon et al., 2010; Marcott et al., 2014; Monnin et al., 2001). Despite this big change in the ocean–atmosphere carbon system, there is very little change in intermediate water $\Delta^{14}C$. The insensitivity of intermediate water $\Delta^{14}C$ to early changes in atmospheric CO_2 indicates, again, that intermediate water is behaving independently from deep water. A comparison of epsilon values from Tasmania to other deglacial radiocarbon records from the Chilean Margin, Drake Passage, deep South Atlantic, and the Chatham Rise, shows this general pattern, with the deepest water getting younger most dramatically at the start of HS1 and shallower water not changing (Fig. 6C, Supplemental Fig. 2) (Burke and Robinson, 2012; De Pol-Holz et al., 2010; Skinner et al., 2015, 2010).

4.2. Rapid variability and zonal asymmetry during the ACR

In the Tasmanian coral $\Delta^{14}C$ record, the ACR stands out compared to the rest of the deglaciation due to its large and abrupt changes in $\Delta^{14}C$, and unprecedented resolution (Fig. 6C). Average sample resolution during the ACR (14.7–12.9 ka) is 55 yr, including 6 corals that have been sub-sampled (excluding the 6 sub-sampled corals decreases the average sample resolution to 105 yr, which is still high compared to most marine records). The variability during this time period is not only seen between corals but also within the lifetimes of several individuals (Fig. 3 and Fig. 6C). Because of the inherent stratigraphy of each skeleton, top middle and bottom dates are able to resolve changes in intermediate water radiocarbon that would otherwise be within calendar age measurement

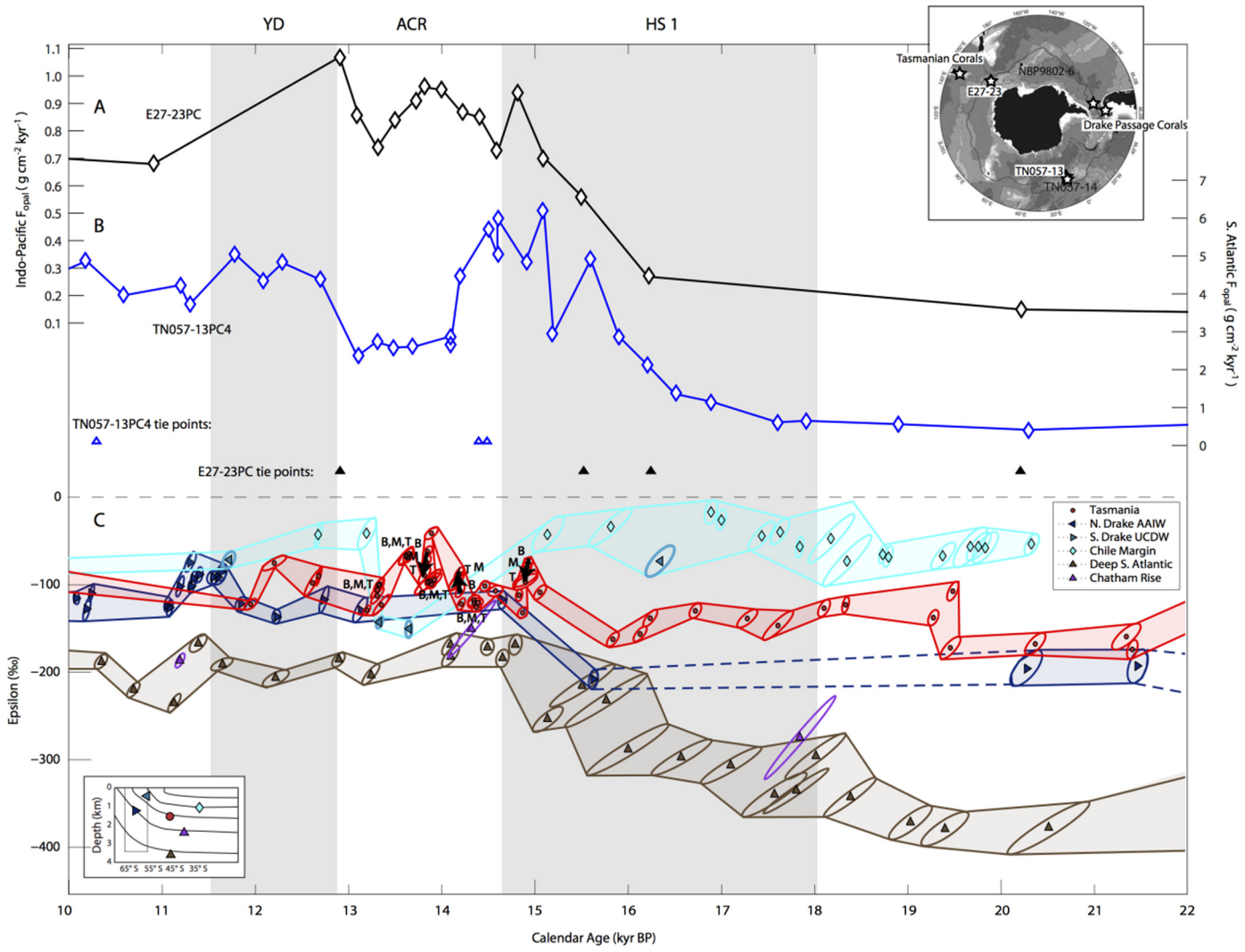

Fig. 6. Opal flux and epsilon radiocarbon records from the Southern Ocean across the deglaciation. A) Opal flux record from Indo-Pacific core E27-23 (59.62°S 155.24°E, 3182 m). B) Opal flux record from South Atlantic core TN057-13 (53.1728°S 5.1275°E, 2848 m). Error bars on opal flux values are the size of the points. Also included are chronological constraints (from calibrated ^{14}C dates) for both cores, with E27-23 tie points in filled black triangles and TN057-13 tie points in open blue triangles. C) Tasmanian coral Δ^{14}C record shown as epsilon units offset from the atmosphere with other Southern Ocean records Δ^{14}C records. Deep South Atlantic (Skinner et al., 2010) (brown ellipses and upward-facing triangles; core MD07-3076; 44.1°S 14.2°E, 4981 m), southern Drake Passage UCDW (Burke and Robinson, 2012) (dark blue ellipses and right-facing triangles; ~60°S, ~1000 m), northern Drake passage AAIW (Burke and Robinson, 2012) (dark teal ellipses and left-facing triangles; ~55°S, 500 m), Chilean Margin (De Pol-Holz et al., 2010) (teal ellipses and diamonds; core SO161-SL22; 36.2°S 73.7°W, 1000 m), Chatham Rise (Skinner et al., 2015) (purple ellipses and upward-facing triangles; core MD97-2121; 40.4°S 178.0°E, 2314 m), and Tasmania (this study) (red ellipses and circles; ~45°S, ~1600 m). "T, M, B" labels refer to top, middle, and bottom Δ^{14}C values for individual corals. Of corals with top, middle, and bottom dates, only three show resolvable changes over the coral's lifespan (see Fig. 3). The direction of these changes is marked with an arrow. Top right: map showing the locations of cores TN057-13 and E27-23, Drake Passage Corals and Tasmanian corals. Bottom left: schematic showing modern Southern Ocean zonally-averaged isopycnal structure, Drake Passage location, and locations of epsilon records (in color-coded symbols). (For interpretation of the references to color in this figure legend, the reader is referred to the web version of this article.)

error. The largest of these jumps occurs at 13.9 ka and has a magnitude of 35‰ over approximately 35 yr. The standard deviation of detrended inter-sample epsilon values during the ACR (i.e. excluding middle and bottom samples) is twice as large as during the LGM and HS1, and a Levene's Test (Levene, 1960) comparing the detrended inter-sample epsilon variability during the ACR to that of the LGM/HS1 rejects the null hypothesis that the variances are equal at the 82% confidence level ($p = 0.177$). It cannot completely be ruled out however, that this difference is the result of the threefold higher sampling resolution during the ACR compared to the LGM/HS1.

The rapidity of these radiocarbon fluctuations implicates frontal shifts, rather than changes in circulation strength, either at the surface or at depth. In the modern ocean south of Tasmania, a 30‰ shift in Δ^{14}C would require fronts to move ~10° latitude based on the surface meridional Δ^{14}C gradient of ~3‰ per degree (Fig. 1). However, some of the inter-sample Δ^{14}C shifts during this time are as large as 80‰, which would require a frontal shift of over 25° latitude based on this same gradient. Given that the Southern Ocean is only about 20° of latitude wide south of Tasmania, it is clearly unreasonable to assume that the surface Δ^{14}C gradient was the same during the ACR. It seems very likely that frontal gradients would have been enhanced during this time because older deep water upwelling around the Antarctic continent would reduce Δ^{14}C values to the south thereby increasing the total gradient across the Southern Ocean. This would decrease the magnitude of SAF/PF shift required to fit our data.

Frontal shifts of 5–10° over the deglaciation have been previously suggested for the Southern Ocean by several different studies (Kohfeld et al., 2013; Sikes et al., 2009). In the most comprehensive frontal reconstructions, shifts of 4–5° have been suggested for the SAF and PF and shifts of 3–5° have been suggested for the

Subtropical Front (STF) (Kohfeld et al., 2013). Differences between the exact location and the temporal resolution of these frontal reconstructions compared to our record makes comparisons of the timing of these frontal shifts less informative than the magnitude of change. There are high-resolution data from south of Australia (De Deckker et al., 2012) through this time period, but the foram abundances indicate that subtropical waters are primarily influencing the core region. Our Tasmanian intermediate water corals are not especially sensitive to Subtropical Front position (NPD percent abundance) or Lewellen Current intensity (*G. ruber* percent abundance), so we do not expect these foram records to be directly comparable to our $\Delta^{14}C$ record during this time period.

Shifts in the position of Southern Ocean fronts, driven by the position of the westerly winds are thought to influence the rate of Southern Ocean upwelling and CO_2 degassing (Anderson et al., 2009; Toggweiler et al., 2006). This is exemplified in the opal flux record from core TN057-13 (53.1728°S 5.1275°E, 2848 m) in the South Atlantic (Anderson et al., 2009). This record shows low opal fluxes during the LGM, consistent with Southern Ocean westerly winds shifted north, outside of the Drake Passage latitude band (Anderson et al., 2009; Toggweiler et al., 2006). At the start of HS1, Northern Hemisphere cooling shifts the westerlies to the south, prompting increased upwelling and higher opal fluxes. This process is reversed at the Bølling–Allerød/ACR, where the Northern Hemisphere warms, and then reversed again at the Younger Dryas, causing a pattern of reduced then increased opal flux (Anderson et al., 2009). Other Southern Ocean records from near this core location highlight the ACR as a time of surface stratification and reduced upwelling (Anderson et al., 2009; Burke and Robinson, 2012; Siani et al., 2013).

During the end of HS1, leading up to the ACR, there seems to be a coherent Southern Ocean response. Upwelling leading to increased opal flux in the South Atlantic (Anderson et al., 2009) and increases in UCDW epsilon values seen in the Drake Passage (Burke and Robinson, 2012) are mirrored by increased opal flux in Indo-Pacific sector core E27-23 (Anderson et al., 2009) (Fig. 6A; 59.62°S 155.24°E, 3182 m) and increases in epsilon south of Tasmania. However, the classic Southern hemisphere pattern of reduced upwelling and enhanced stratification during the middle of the ACR, typified by the South Atlantic opal flux record, is distinctly different from the pattern seen in the Indo-Pacific sector core (Fig. 6A, B). In E27-23 there is upwelling throughout the ACR with some amount of temporal variability. It is tempting to look for a correlation between the Indo-Pacific opal flux record, as an indicator of front position, and the rapid, short-timescale variability in the Tasmanian coral epsilon record. Indeed the Indo-Pacific opal flux and Tasmanian coral epsilon records do seem to line up, however the age model for Indo-Pacific core E27-23 is much less well constrained than that of South Atlantic core TN057-13. There are three calendar age tie points for E27-23 between 12–17 ka, so if the opal flux data from E27-23 were shifted to better match the patterns in TN057-13, it would require two abrupt changes in sedimentation rate during this time period. The observation that Indo-Pacific opal fluxes do not look the same as South Atlantic opal fluxes, and their close correspondence with the Tasmanian coral $\Delta^{14}C$, indicates that there is zonal asymmetry across the Southern Ocean during the ACR.

Although the Drake Passage UCDW record looks quite similar to our Tasmanian coral record during the end of HS1, a comparison of Tasmanian coral epsilon values to both the UCDW and AAIW records from Drake Passage during this time shows potential differences (Fig. 6C). This is most obvious at ~13.6 ka, where one Drake Passage AAIW sample falls almost 100‰ below the contemporaneous Tasmanian coral samples. The Drake Passage corals more closely resemble the South Atlantic opal flux record, while the Tasmanian corals more closely resemble the Indo-Pacific opal flux record (Fig. 6), despite the fact that the Tasmanian record should fall between the two Drake Passage records according to a zonally symmetric view of the modern hydrography (Fig. 6, inset at lower left). Drake Passage is unique in the Southern Ocean, as it steers all the volume of the ACC and many of the Southern Ocean fronts through a fairly narrow channel, so one might expect fronts to behave differently in this region than they would south of Tasmania. Although there are some important topographic features south of Tasmania, such as the Tasman Plateau, this primarily influences the position of the Subtropical Front, leaving the Subantarctic and Polar Fronts free to move. It is also important to note that the discrepancy between the Drake Passage and Tasmanian coral records is largely driven by a gap in the UCDW record between 14.7–13.1 ka, so it is also possible that apparent zonal differences are simply driven by a lack of temporal overlap between the records. For the foraminiferal records (De Pol-Holz et al., 2010; Skinner et al., 2015, 2010), fronts near the Chile Margin and Chatham Rise should be less affected by topography than those in the Southeast Atlantic, however sampling gaps make it impossible to determine the extent to which frontal movement influences $\Delta^{14}C$ values at these locations.

4.3. Intermediate water perspectives on deglacial overturning circulation

One of the strongest climate signals through the deglaciation is the rise in atmospheric CO_2 and its connection with Southern Hemisphere warming and deep ocean ventilation (Fig. 7C, D, F) (Marcott et al., 2014; Skinner et al., 2010; WAIS Divide Project Members, 2013). On top of this broad signal there are abrupt ~12 ppm rises in pCO_2 at ~16 ka and ~14.7 ka (Marcott et al., 2014). This first abrupt CO_2 increase occurs at about the same time as Heinrich Event 1 and the associated maximum weak monsoon interval seen in the Hulu cave record (Fig. 7B) (Wang et al., 2001). This interval is thought to be associated with a southward shift of the ITCZ and other atmospheric wind systems (McGee et al., 2014), which should show up in Tasmanian intermediate water $\Delta^{14}C$ as a positive shift in epsilon values. Instead intermediate water $\Delta^{14}C$ gets gradually older.

This somewhat surprising observation could be the result of mechanism 2 in Fig. 1C—at this time there is convergence between deeper and shallower water masses (Fig. 7F) (Burke and Robinson, 2012), indicating that the deep overturning cells have become temporarily more interconnected. After this convergence, there is a pause in atmospheric CO_2 rise, indicating less ventilation of deep water, perhaps due to expanded sea ice, which shoals the boundary between the upper and lower cells and reduces mixing between intermediate and deep waters. Without the influence of old deep water, Tasmanian intermediate water $\Delta^{14}C$ returns to the value dictated by the position of the fronts in the Southern Ocean (Fig. 7E). At ~15 ka, the ITCZ starts to move north and intermediate water epsilon values drop.

At the start of the Bølling, there is another 12 ppm increase in atmospheric CO_2. This could be the result of deep convection in the North Atlantic, possibly associated with thermobaric capacitance and stored heat at mid-depths (Thiagarajan et al., 2014). There is also a slight convergence of intermediate and deeper waters in the Southern Ocean at this time, so perhaps there is also a southern source to this atmospheric CO_2 rise. During the rest of the ACR and Bølling–Allerød, atmospheric CO_2 stays constant and Antarctic $\delta^{18}O$ drops (Fig. 7C, D, F). Intermediate water $\Delta^{14}C$, on the other hand, is highly variable and generally younger than earlier in the deglaciation. As indicated by the constant pCO_2, there is separation between the upper and lower circulation cells, while intermediate waters respond to atmospheric forcing unbuffered by mixing of deeper and older waters.

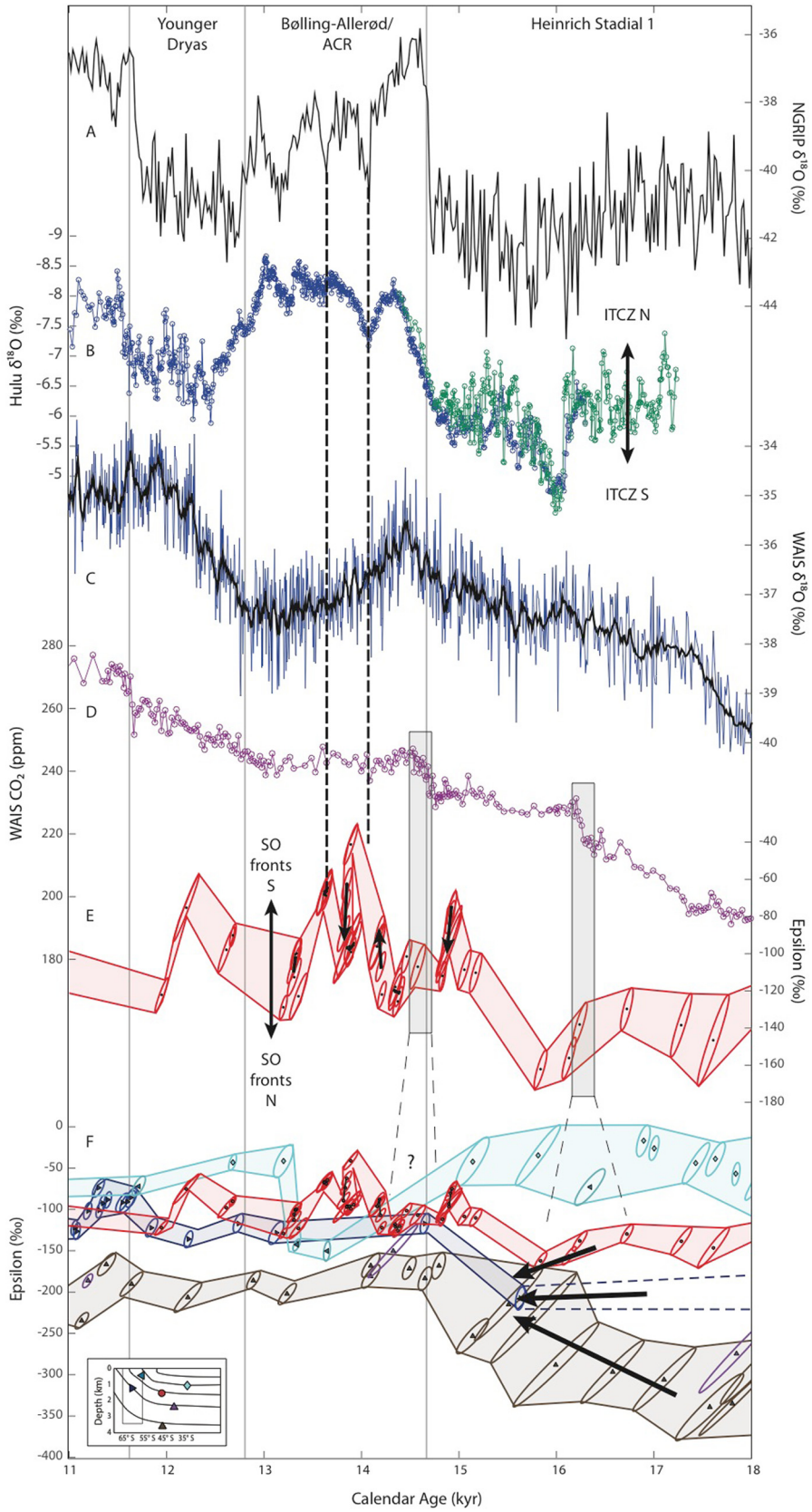

Fig. 7. Records of the full deglacial period showing changes in overturning circulation. A) NGRIP δ^{18}O from Greenland (Andersen et al., 2006; Rasmussen et al., 2006). B) Hulu cave δ^{18}O from stalagmites H82 (blue) and YT (green) (Wang et al., 2001). C) WAIS Divide δ^{18}O from west Antarctica (WAIS Divide Project Members, 2013). D) Atmospheric CO_2 from WAIS Divide (Marcott et al., 2014). E) Δ^{14}C record from south of Tasmania represented as epsilon (this study). F) Tasmanian Δ^{14}C record with other Southern Ocean Δ^{14}C records (same colors and symbols as Fig. 6C) (Burke and Robinson, 2012; De Pol-Holz et al., 2010; Skinner et al., 2015, 2010). (For interpretation of the references to color in this figure legend, the reader is referred to the web version of this article.)

If the rapid fluctuations in Tasmanian coral $\Delta^{14}C$ record during the ACR/Bølling–Allerød are due to frontal movement in the Southern Ocean, then the question of what drives these shifts arises. Antarctic $\delta^{18}O$ drops during the ACR, but there is no resolvable second-order variability on top of the broader shift in isotope value (Fig. 7C). On the other hand, there is structure within the Greenland $\delta^{18}O$ record during the Bølling–Allerød (Fig. 7A). During the early part of the ACR/Bølling, there is some correspondence between Greenland $\delta^{18}O$ and Tasmanian coral $\Delta^{14}C$, as illustrated by vertical dashed lines in Fig. 7. By the same mechanism previously discussed to explain the frontal shift at 19 ka, a sharp drop in Greenland $\delta^{18}O$ should shift winds and fronts to the south and lead to an increase in Tasmanian coral epsilon. While this correspondence between Tasmanian coral epsilon and Greenland $\delta^{18}O$ holds for the first two sharp drops (at 14.1 and 13.6 ka), by about 13.3 ka Southern Ocean intermediate water records have converged again and there is no longer a connection between Tasmanian corals and Greenland, though there is a slight gap in the coral record at this time.

4.4. Other times of intermediate water variability

The earliest part of the Tasmanian coral $\Delta^{14}C$ record is also characterized by rapid, albeit more ambiguous, variability. This variability directly contrasts with the LGM section of the record where intermediate water $\Delta^{14}C$ clearly follows the atmosphere, and indicates that the ocean is most likely not in steady state during this interval (~28–23 ka). The timing of variability and non-steady state behavior seen early in the Tasmanian coral record is not surprising, however, since it follows the transition between Marine Isotope Stages 3 and 2 (Lisiecki and Raymo, 2005). Around 25 ka in particular there is a large range of $\Delta^{14}C$ values. While this spread in $\Delta^{14}C$ may be driven by the same mechanisms that lead to intermediate water variability later in the record, it is difficult to resolve specific changes in intermediate water radiocarbon due to uncertainty in the radiocarbon dates driven by error associated with deep-sea coral blanks (Supplemental Fig. 1). Therefore, it is hard to determine a specific forcing or mechanism for $\Delta^{14}C$ change. It is worth noting that two of the earliest samples in the record overlap with the IntCal13 atmospheric $\Delta^{14}C$ record. This is quite unusual due to old surface reservoir ages in the Southern Ocean, however there is a great deal of scatter among the datasets that comprise the IntCal13 atmospheric $\Delta^{14}C$ compilation during this time period, so the apparent overlap between our record and the atmosphere is not necessarily representative of intermediate water of zero age.

Probably the most striking feature of the record during this time is the ~250‰ drop in intermediate water $\Delta^{14}C$ between 27.6–26.2 ka. The trajectory of this drop closely matches that of ^{14}C decay, implicating in situ ageing of a water mass. It also closely matches the initial portion of a $\Delta^{14}C$ drop from the Brazil Margin observed by Mangini et al. starting at 27.9 ka (Supplemental Fig. 3) (Mangini et al., 2010). Mangini et al. suggest that this drop in intermediate water $\Delta^{14}C$ is related to a slowdown in the meridional overturning circulation during Heinrich 2. Yet a circulation slowdown that would give decay-like $\Delta^{14}C$ trajectories implies complete stagnation of the water, or an unlikely mixing scenario between multiple water masses. In addition, deep circulation changes in the North Atlantic and southern sourced intermediate waters are not expected to be in phase if the 'seesaw' mechanism (Broecker, 1998) is still at work during this time. Another possible mechanism is mixing with ^{14}C-dead water. While it would be difficult to simulate a decay-like $\Delta^{14}C$ trajectory by mixing water masses that contain radiocarbon, a 50:50 mixture with ^{14}C-dead water over 5730 yr naturally mimics decay. If mixing with ^{14}C-dead water was the cause of the decay-like drop in $\Delta^{14}C$ at ~27.6 ka, however, the source of this water remains elusive.

The 250‰$\Delta^{14}C$ drop at 27.6 ka is similar in magnitude to some of the intermediate water variability observed during the ACR. However, the high-resolution data during the deglaciation clearly distinguish the intermediate water changes from the stagnation signature of ^{14}C decay. It is therefore not hard to imagine that higher-resolution data at 27.6 ka might also differentiate this three-point $\Delta^{14}C$ drop from a decay trajectory. Likewise, more data could potentially change the interpretation of the Brazil Margin record, however, the longer duration of each stagnation event and repetition of decay trajectories over their entire interval sets their dataset apart from the alternating variability and steady–state behavior observed in our intermediate water record.

5. Conclusion

Our high-resolution $\Delta^{14}C$ record from south of Tasmania highlights times during the deglaciation when the upper and lower cells of the MOC are more or less interconnected. It also emphasizes the importance of fronts in the Southern Ocean for determining the radiocarbon values and short-term variability of intermediate waters.

During much of the Last Glacial Maximum we see evidence for steady state circulation. Tasmanian intermediate water $\Delta^{14}C$ follows the contemporaneous atmosphere, and production-corrected atmospheric $\Delta^{14}C$ is nearly constant in time. There is however one obvious departure from steady–state at around 19 ka, where a 10–15 m sea level rise (Yokoyama et al., 2000) is accompanied by a southward shift of the Subantarctic and Polar Fronts (De Deckker et al., 2012) and a 40‰ rise in intermediate water $\Delta^{14}C$. This abrupt shift only impacts the upper cell however—production-corrected atmospheric $\Delta^{14}C$ values and atmospheric CO_2 are unaffected.

Intermediate water south of Tasmania is much more dynamic beginning late in HS1 and continuing through the Antarctic Cold Reversal. Fronts are aligned with the large-scale density structure of the Southern Ocean, and because of the pattern of upwelling, these fronts are also aligned with radiocarbon gradients. Frontal position is strongly influenced by topography (Graham et al., 2012), but in the absence of large topographic features, fronts are free to move in response to Southern Ocean westerly winds (Sallée et al., 2008). Although on a large scale the Southern Ocean is zonally symmetric there is important regional variability, largely driven by topography. This zonal asymmetry helps explain why Tasmanian intermediate water $\Delta^{14}C$ and Indo-Pacific upwelling records deviate from similar South Atlantic records (Anderson et al., 2009; Burke and Robinson, 2012; De Pol-Holz et al., 2010; Skinner et al., 2015, 2010).

Tasmanian intermediate water $\Delta^{14}C$ shows that the classic view of weakened overturning in the Southern Ocean during the Antarctic Cold Reversal is not appropriate for all regions. The timing of intermediate water $\Delta^{14}C$ variability south of Tasmania during parts of the ACR matches with $\delta^{18}O$ values measured in Greenland ice and Chinese speleothems. This upper cell variability and connection to Northern Hemisphere records indicates a separation between the circulation cells and less of a deep water influence at the sample location during this time. Earlier in the deglaciation, at ~16 ka, atmospheric signals associated with Heinrich Event 1 are not immediately seen in Tasmanian intermediate waters because they are overprinted by the effects of mixing with old deeper water masses. By the end of the ACR, overturning circulation more closely matches the modern and intermediate and deep water masses are organized accordingly.

Early in the record, following the Marine Isotope Stage 3–2 transition at 29 ka, there is also a great deal of variability in

intermediate water $\Delta^{14}C$, however it is more difficult to resolve clear patterns and connect them to specific forcings. One discernable feature is a 1400-yr 250‰ drop starting at 27.6 ka, which closely follows the trajectory of ^{14}C decay. This $\Delta^{14}C$ drop corresponds to the first half of a drop observed off the coast of Brazil (Mangini et al., 2010). We hesitate to interpret our signal as intermediate water stagnation since it is difficult to imagine physical mechanisms wherein this could be achieved. The magnitude of this drop is similar to some of the variability observed during the ACR section of the record. Whereas the high-resolution data during the deglaciation clearly distinguish intermediate water $\Delta^{14}C$ variability from ^{14}C decay, the lack of data density at 27.6 ka makes this distinction difficult. More $\Delta^{14}C$ measurements could lead to a better understanding of the mechanisms at play during this time period, but we recovered few corals that grew during this time.

Acknowledgements

We would like to thank Heather Stoll, the editor of this paper, and three reviewers for their helpful comments. We would also like to acknowledge analytical help from Guillaume Paris. This work was funded by NSF P2C2 grant OCE-1204211.

Appendix A. Supplementary material

Supplementary material related to this article can be found online at http://dx.doi.org/10.1016/j.epsl.2015.09.038.

References

Adkins, J.F., Griffin, S., Kashgarian, M., Cheng, H., Druffel, E.R.M., Boyle, E.A., Edwards, R.L., Shen, C.-C., 2002. Radiocarbon dating of deep-sea corals. Radiocarbon 44, 567–580.

Adkins, J.F., Henderson, G.M., Wang, S.L., O'Shea, S., Mokadem, F., 2004. Growth rates of the deep-sea scleractinia Desmophyllum cristagalli and Enallopsammia rostrata. Earth Planet. Sci. Lett. 227, 481–490. http://dx.doi.org/10.1016/j.epsl.2004.08.022.

Andersen, K.K., Svensson, A., Johnsen, S.J., Rasmussen, S.O., Bigler, M., Rothlisberger, R., Ruth, U., Siggaard-Andersen, M.-L., Peder Steffensen, J., Dahl-Jensen, D., 2006. The Greenland ice core chronology 2005, 15–42 ka. Part 1: constructing the time scale. Quat. Sci. Rev. 25, 3246–3257. http://dx.doi.org/10.1016/j.quascirev.2006.08.002.

Anderson, R.F., Ali, S., Bradtmiller, L.I., Nielsen, S.H.H., Fleisher, M.Q., Anderson, B.E., Burckle, L.H., 2009. Wind-driven upwelling in the Southern Ocean and the deglacial rise in atmospheric CO_2. Science 323, 1443–1448. http://dx.doi.org/10.1126/science.1167441.

Broecker, W.S., 1998. Paleocean circulation during the last deglaciation: a bipolar seesaw? Paleoceanography 13, 119–121.

Burke, A., Robinson, L.F., 2012. The Southern Ocean's role in carbon exchange during the last deglaciation. Science 335, 557–561. http://dx.doi.org/10.1126/science.1208163.

Burke, A., Robinson, L.F., McNichol, A.P., Jenkins, W.J., Scanlon, K.M., Gerlach, D.S., 2010. Reconnaissance dating: a new radiocarbon method applied to assessing the temporal distribution of Southern Ocean deep-sea corals. Deep-Sea Res., Part 1 57, 1510–1520. http://dx.doi.org/10.1016/j.dsr.2010.07.010.

Bush, S.L., Santos, G.M., Xu, X., Southon, J.R., Thiagarajan, N., Hines, S.K., Adkins, J.F., 2013. Simple, rapid, and cost effective: a screening method for ^{14}C analysis of small carbonate samples. Radiocarbon 55, 631–640. http://dx.doi.org/10.2458/azu_js_rc.55.16192.

Ceppi, P., Hwang, Y.T., Liu, X., Frierson, D.M.W., Hartmann, D.L., 2013. The relationship between the ITCZ and the Southern Hemispheric eddy-driven jet. J. Geophys. Res., Atmos. 118, 1–11.

Cheng, H., Adkins, J., Edwards, R.L., Boyle, E.A., 2000. U–Th dating of deep-sea corals. Geochim. Cosmochim. Acta 64, 2401–2416.

Clark, P.U., Dyke, A.S., Shakun, J.D., Carlson, A.E., Clark, J., Wohlfarth, B., Mitrovica, J.X., Hostetler, S.W., McCabe, A.M., 2009. The last glacial maximum. Science 325, 710–714. http://dx.doi.org/10.1126/science.1172873.

Curry, W.B., Oppo, D.W., 2005. Glacial water mass geometry and the distribution of $\delta^{13}C$ of ΣCO_2 in the western Atlantic Ocean. Paleoceanography 20, PA1017. http://dx.doi.org/10.1029/2004PA001021.

De Deckker, P., Moros, M., Perner, K., Jansen, E., 2012. Influence of the tropics and southern westerlies on glacial interhemispheric asymmetry. Nat. Geosci. 5, 266–269. http://dx.doi.org/10.1038/ngeo1431.

De Pol-Holz, R., Keigwin, L., Southon, J., Hebbeln, D., Mohtadi, M., 2010. No signature of abyssal carbon in intermediate waters off Chile during deglaciation. Nat. Geosci. 3, 192–195. http://dx.doi.org/10.1038/ngeo745.

Eltgroth, S.F., Adkins, J.F., Robinson, L.F., Southon, J., Kashgarian, M., 2006. A deep-sea coral record of North Atlantic radiocarbon through the Younger Dryas: evidence for intermediate water/deepwater reorganization. Paleoceanography 21. http://dx.doi.org/10.1029/2005PA001192.

Ferrari, R., Jansen, M.F., Adkins, J.F., Burke, A., Stewart, A.L., Thompson, A.F., 2014. Antarctic sea ice control on ocean circulation in present and glacial climates. Proc. Natl. Acad. Sci. USA 111, 8753–8758. http://dx.doi.org/10.1073/pnas.1323922111.

Graham, R.M., De Boer, A.M., Heywood, K.J., Chapman, M.R., Stevens, D.P., 2012. Southern Ocean fronts: controlled by wind or topography? J. Geophys. Res., Atmos. 117. http://dx.doi.org/10.1029/2012JC007887.

Hain, M.P., Sigman, D.M., Haug, G.H., 2014. Distinct roles of the Southern Ocean and North Atlantic in the deglacial atmospheric radiocarbon decline. Earth Planet. Sci. Lett. 394, 198–208. http://dx.doi.org/10.1016/j.epsl.2014.03.020.

Indermühle, A., Monnin, E., Stauffer, B., Stocker, T.F., Wahlen, M., 2000. Atmospheric CO_2 concentration from 60 to 20 kyr BP from the Taylor Dome Ice Core, Antarctica. Geophys. Res. Lett. 27, 735–738. http://dx.doi.org/10.1029/1999GL010960.

Kang, S.M., Held, I.M., Frierson, D.M.W., Zhao, M., 2008. The response of the ITCZ to extratropical thermal forcing: idealized slab-ocean experiments with a GCM. J. Climate 21, 3521–3532. http://dx.doi.org/10.1175/2007JCLI2146.1.

Key, R., Kozyr, A., Sabine, C., Lee, K., Wanninkhof, R., Bullister, J., Feely, R., Millero, F., Mordy, C., Peng, T., 2004. A global ocean carbon climatology: results from Global Data Analysis Project (GLODAP). Glob. Biogeochem. Cycles 18. http://dx.doi.org/10.1029/2004GB002247.

Knox, F., McElroy, M.B., 1984. Changes in atmospheric CO_2: influence of the marine biota at high latitude. J. Geophys. Res., Atmos. 89, 4629. http://dx.doi.org/10.1029/JD089iD03p04629.

Kohfeld, K.E., Graham, R.M., de Boer, A.M., Sime, L.C., Wolff, E.W., Le Quere, C., Bopp, L., 2013. Southern Hemisphere westerly wind changes during the Last Glacial Maximum: paleo-data synthesis. Quat. Sci. Rev. 68, 76–95. http://dx.doi.org/10.1016/j.quascirev.2013.01.017.

Laj, C., Kissel, C., Mazaud, A., Michel, E., 2002. Geomagnetic field intensity, North Atlantic Deep Water circulation and atmospheric $\Delta^{14}C$ during the last 50 kyr. Earth Planet. Sci. Lett. 200, 177–190.

Lemieux-Dudon, B., Blayo, E., Petit, J.-R., Waelbroeck, C., Svensson, A., Ritz, C., Barnola, J.-M., Narcisi, B.M., Parrenin, F., 2010. Quaternary science reviews. Quat. Sci. Rev. 29, 8–20. http://dx.doi.org/10.1016/j.quascirev.2009.11.010.

Levene, H., 1960. Robust test for equality of variances. In: Olkin, I., Ghurye, S.G., Hoeffding, W. (Eds.), Contributions to Probability and Statistics: Essays in Honour of Harold Hotelling. Stanford University Press, Stanford, pp. 278–292.

Lisiecki, L.E., Raymo, M.E., 2005. A Pliocene–Pleistocene stack of 57 globally distributed benthic $\delta^{18}O$ records. Paleoceanography 20. http://dx.doi.org/10.1029/2004PA001071.

Lund, D.C., Adkins, J.F., Ferrari, R., 2011. Abyssal Atlantic circulation during the Last Glacial Maximum: constraining the ratio between transport and vertical mixing. Paleoceanography 26. http://dx.doi.org/10.1029/2010PA001938.

Mangini, A., Godoy, J.M., Godoy, M.L., Kowsmann, R., Santos, G.M., Ruckelshausen, M., Schroeder-Ritzrau, A., Wacker, L., 2010. Deep sea corals off Brazil verify a poorly ventilated Southern Pacific Ocean during H2, H1 and the Younger Dryas. Earth Planet. Sci. Lett. 293, 269–276. http://dx.doi.org/10.1016/j.epsl.2010.02.041.

Marcott, S.A., Bauska, T.K., Buizert, C., Steig, E.J., Rosen, J.L., Cuffey, K.M., Fudge, T.J., Severinghaus, J.P., Ahn, J., Kalk, M.L., McConnell, J.R., Sowers, T., Taylor, K.C., White, J.W.C., Brook, E.J., 2014. Centennial-scale changes in the global carbon cycle during the last deglaciation. Nature 514, 616–619.

McGee, D., Donohoe, A., Marshall, J., Ferreira, D., 2014. Changes in ITCZ location and cross-equatorial heat transport at the Last Glacial Maximum, Heinrich Stadial 1, and the mid-Holocene. Earth Planet. Sci. Lett. 390, 69–79. http://dx.doi.org/10.1016/j.epsl.2013.12.043.

Monnin, E., Indermühle, A., Dällenbach, A., Flückiger, J., Stauffer, B., Stocker, T.F., Raynaud, D., Barnola, J.-M., 2001. Atmospheric CO_2 concentrations over the last glacial termination. Science 291, 112–114. http://dx.doi.org/10.1126/science.291.5501.112.

Muscheler, R., Beer, J., Wagner, G., Laj, C., Kissel, C., Raisbeck, G., Yiou, F., Kubik, P., 2004. Changes in the carbon cycle during the last deglaciation as indicated by the comparison of ^{10}Be and ^{14}C records. Earth Planet. Sci. Lett. 219, 325–340.

Rasmussen, S.O., Andersen, K.K., Svensson, A.M., Steffensen, J.P., Vinther, B., Clausen, H.B., Siggaard-Andersen, M.-L., Johnsen, S.J., Larsen, L.B., Dahl-Jensen, D., Bigler, M., Rothlisberger, R., Fischer, H., Goto-Azuma, K., Hansson, M., Ruth, U., 2006. A new Greenland ice core chronology for the last glacial termination. J. Geophys. Res., Atmos. 111.

Reimer, P.J., Baillie, M.G.L., Bard, E., Bayliss, A., Beck, J.W., Blackwell, P.G., Ramsey, C.B., Buck, C.E., Burr, G.S., Edwards, R.L., Friedrich, M., Grootes, P.M., Guilderson, T.P., Hajdas, I., Heaton, T.J., Hogg, A.G., Hughen, K.A., Kaiser, K.F., Kromer, B., McCormac, F.G., Manning, S.W., Reimer, R.W., Richards, D.A., Southon, J.R., Talamo, S., Turney, C.S.M., van der Plicht, J., Weyhenmeyer, C.E., 2009. IntCal09 and Marine09 radiocarbon age calibration curves, 0–50,000 years cal BP. Radiocarbon 51, 1111–1150.

Robinson, L.F., Adkins, J.F., Scheirer, D.S., Fernandez, D.P., Gagnon, A.C., Waller, R.G., 2007. Deep-sea scleractinian coral age and depth distributions in the WN Atlantic for the last 225 thousand years. Bull. Mar. Sci. 81, 371–391.

Rose, K.A., Sikes, E.L., Guilderson, T.P., Shane, P., Hill, T.M., Zahn, R., Spero, H.J., 2010. Upper-ocean-to-atmosphere radiocarbon offsets imply fast deglacial carbon dioxide release. Nature 466, 1093–1097. http://dx.doi.org/10.1038/nature09288.

Sallée, J.B., Speer, K., Morrow, R., 2008. Response of the Antarctic Circumpolar Current to atmospheric variability. J. Climate 21, 3020–3039. http://dx.doi.org/10.1175/2007JCLI1702.1.

Santos, G.M., Mazon, M., Southon, J.R., Rifai, S., Moore, R., 2007. Evaluation of iron and cobalt powders as catalysts for ^{14}C-AMS target preparation. Nucl. Instrum. Methods Phys. Res., Sect. B, Beam Interact. Mater. Atoms 259, 308–315. http://dx.doi.org/10.1016/j.nimb.2007.01.220.

Sarmiento, J.L., Toggweiler, J.R., 1984. A new model for the role of the oceans in determining atmospheric pCO_2. Nature 308, 621–624.

Shakun, J.D., Clark, P.U., He, F., Marcott, S.A., Mix, A.C., Liu, Z., Otto-Bliesner, B., Schmittner, A., Bard, E., 2012. Global warming preceded by increasing carbon dioxide concentrations during the last deglaciation. Nature 484, 49–54. http://dx.doi.org/10.1038/nature10915.

Shen, G.T., Boyle, E.A., 1988. Determination of lead, cadmium and other trace metals in annually-banded corals. Chem. Geol. 67, 47–62. http://dx.doi.org/10.1016/0009-2541(88)90005-8.

Siani, G., Michel, E., De Pol-Holz, R., DeVries, T., Lamy, F., Carel, M.E.L., Isguder, G., Dewilde, F., Lourantou, A., 2013. Carbon isotope records reveal precise timing of enhanced Southern Ocean upwelling during the last deglaciation. Nat. Commun. 4, 1–9. http://dx.doi.org/10.1038/ncomms3758.

Siegenthaler, U., Wenk, T., 1984. Rapid atmospheric CO_2 variations and ocean circulation. Nature 308, 624–626. http://dx.doi.org/10.1038/308624a0.

Sigman, D.M., Hain, M.P., Haug, G.H., 2010. The polar ocean and glacial cycles in atmospheric CO_2 concentration. Nature 466, 47–55. http://dx.doi.org/10.1038/nature09149.

Sikes, E.L., Howard, W.R., Samson, C.R., Mahan, T.S., Robertson, L.G., Volkman, J.K., 2009. Southern Ocean seasonal temperature and Subtropical Front movement on the South Tasman Rise in the late Quaternary. Paleoceanography 24. http://dx.doi.org/10.1029/2008PA001659.

Skinner, L., McCave, I.N., Carter, L., Fallon, S., Scrivner, A.E., Primeau, F., 2015. Reduced ventilation and enhanced magnitude of the deep Pacific carbon pool during the last glacial period. Earth Planet. Sci. Lett. 411, 45–52. http://dx.doi.org/10.1016/j.epsl.2014.11.024.

Skinner, L.C., Fallon, S., Waelbroeck, C., Michel, E., Barker, S., 2010. Ventilation of the deep Southern Ocean and deglacial CO_2 rise. Science 328, 1147–1151. http://dx.doi.org/10.1126/science.1183627.

Stuiver, M., Polach, H.A., 1977. Reporting of C-14 data—discussion. Radiocarbon 19, 355–363.

Talley, L., 2013. Closure of the global overturning circulation through the Indian, Pacific, and Southern Oceans: schematics and transports. Oceanography 26, 80–97. http://dx.doi.org/10.5670/oceanog.2013.07.

Talley, L.D., 2003. Shallow, intermediate, and deep overturning components of the global heat budget. J. Phys. Oceanogr. 33, 530–560.

Thiagarajan, N., Gerlach, D., Roberts, M.L., Burke, A., McNichol, A.P., Jenkins, W.J., Subhas, A., Thresher, R., Adkins, J., 2013. Movement of deep-sea coral populations on climatic timescales. Paleoceanography 28, 227–236.

Thiagarajan, N., Subhas, A.V., Southon, J.R., Eiler, J.M., 2014. Abrupt pre-Bolling-Allerod warming and circulation changes in the deep ocean. Nature 511, 75–78. http://dx.doi.org/10.1038/nature13472.

Toggweiler, J.R., Russell, J.L., Carson, S.R., 2006. Midlatitude westerlies, atmospheric CO_2, and climate change during the ice ages. Paleoceanography 21. http://dx.doi.org/10.1029/2005PA001154.

WAIS Divide Project Members, 2013. Onset of deglacial warming in West Antarctica driven by local orbital forcing. Nature 500, 440–444. http://dx.doi.org/10.1038/nature12376.

Wang, Y.J., Cheng, H., Edwards, R.L., An, Z.S., Wu, J.Y., Shen, C.-C., Dorale, J.A., 2001. A high-resolution absolute-dated late Pleistocene monsoon record from Hulu Cave, China. Science 294, 2345–2348. http://dx.doi.org/10.1126/science.1064618.

Yokoyama, Y., Lambeck, K., De Deckker, P., Johnston, P., Fifield, L.K., 2000. Timing of the Last Glacial Maximum from observed sea-level minima. Nature 406, 713–716.